EurJIC European Journal of Inorganic Chemistry

ChemPubSoc Europe

FULL PAPER

DOI:10.1002/ejic.201300048

Benzo[*c*]thiophene Chromophores Linked to Cationic Fe and Ru Derivatives for NLO Materials: Synthesis Characterization and Quadratic Hyperpolarizabilities

Tiago J. L. Silva,[a] Paulo J. Mendes,*[b] M. Helena Garcia,[a] M. Paula Robalo,[c,d] J. P. Prates Ramalho,[b] A. J. Palace Carvalho,[b] Marina Büchert,[e] Christian Wittenburg,[e] and Jürgen Heck[e]

Keywords: Ruthenium / Iron / Sulfur heterocycles / Nonlinear optics / Hyperpolarizabilities

η^5-Monocyclopentadienyliron(II)/ruthenium(II) complexes of the general formula $[M(\eta^5\text{-}C_5H_5)(PP)(L\mathbf{1})][PF_6]$ {M = Fe, PP = dppe; M = Ru, PP = dppe or $2PPh_3$; L**1** = 5-[3-(thiophen-2-yl)-benzo[*c*]thiophenyl]thiophene-2-carbonitrile} have been synthesized and studied to evaluate their molecular quadratic hyperpolarizabilities. The compounds were fully characterized by NMR, FTIR and UV/Vis spectroscopy and their electrochemical behaviour studied by cyclic voltammetry. Quadratic hyperpolarizabilities (β) were determined by hyper-Rayleigh scattering measurements at a fundamental wavelength of 1500 nm. Density functional theory calculations were employed to rationalize the second-order non-linear optical properties of these complexes.

Introduction

The exploitation of organometallic chemistry for the synthesis of compounds with non-linear optical (NLO) properties has been mainly motivated by their use in optical devices.[1] During the last two decades, significant work has been published outlining the most important progress in the field.[2–11] According to the overall results, the general understanding is that second-order non-linearities are strongly related to asymmetric push–pull systems. In the case of organometallic compounds, the metal centre can be bound to a highly polarizable conjugated backbone, thereby acting as an electron-releasing or -withdrawing group. This type of structural feature leads to large quadratic hyperpolarizabilities arising from intense low-energy metal-to-ligand charge transfer (MLCT), ligand-to-metal charge transfer (LMCT) or intraligand charge transfer (ILCT) excitations. Among the organometallic compounds presenting this structural feature, our group and others have carried out systematic studies on η^5-monocyclopentadienylmetal complexes with benzene or oligothiophene conjugated chains coordinated to the metal centres through nitrile or acetylide linkages.[8,12–18] In particular, very efficient NLO responses were found when strong electron donors such as iron and ruthenium organometallic moieties were coupled with strong electron acceptors like NO_2.

Although fundamental research on NLO properties has mostly been devoted to the preparation of compounds with large optical non-linearities, the use of these properties in molecular switching has attracted considerable interest.[19–29] Organotransition-metal compounds revealed encouraging results because the presence of a redox-active metal centre within a conjugated system provides excellent opportunities for reversible modulation of the second-order non-linear optical (SONLO) properties. Our on-going work in this field was motivated by benzo[*c*]thiophene-based chromophores, the unique electronic behaviour of which, originating from their low HOMO–LUMO energy gaps,[30,31] can potentially yield interesting NLO effects. A soluble form of polyisothianaphthene was found to originate a large third-order non-linear optical response[32] and a ferrocenylethenyl-thienyl-2-thienylbenzo[*c*]thiophene organometallic complex exhibits moderate quadratic hyperpolarizabilities.[33] However, the structure of this metallocene derivative, in which the metal is placed orthogonally

[a] Centro de Ciências Materiais e Moleculares, Faculdade de Ciências da Universidade de Lisboa,
Campo Grande, 1749-016 Lisboa, Portugal
[b] Centro de Química de Évora,
Rua Romão Ramalho 59, 7002-554 Évora, Portugal
Fax: +351-266745303
E-mail: pjgm@uevora.pt
Homepage: www.cqe.uevora.pt/
[c] Centro de Química Estrutural, Instituto Superior Técnico, Universidade Técnica de Lisboa,
Av. Rovisco Pais, 1049-001 Lisboa, Portugal
[d] Área Departamental de Engenharia Química, Instituto Superior de Engenharia de Lisboa,
Rua Conselheiro Emídio Navarro 1, 1959-007 Lisboa, Portugal
[e] Institut für Anorganische und Angewandte Chemie, Universität Hamburg,
Martin-Luther-King-Platz 6, 20146 Hamburg, Germany

Supporting information for this article is available on the WWW under http://dx.doi.org/10.1002/ejic.201300048.

to the extended π system, does not favour better coupling between the organometallic fragment and the conjugated chromophore to achieve high quadratic hyperpolarizabilities. Comparing the metallocene systems that have been studied for NLO purposes, the main structural feature of our η^5-monocyclopentadienylmetal complexes is the presence of the metal centre in the same plane as the π system, this allowing better coupling between the organometallic fragment and the conjugated chromophores. Recently we performed DFT calculations to investigate the quadratic hyperpolarizabilities of η^5-monocyclopentadienyliron(II) and -ruthenium(II) model complexes with 5-[3-(thiophen-2-yl)benzo[*c*]thiophenyl]thiophene-2-carbonitrile as a ligand to evaluate their potential applications as SONLO switches.[34] Based on previous reports that higher hyperpolarizabilities can be achieved upon oxidation and/or reduction, our motivation in that work was to study molecules with architectural features different to the traditional D–π–A system. We adopted a more likely less studied D–π–D′ feature ("off" form), from which a D–π–A′ structure ("on" form) can be achieved upon oxidation and hence an expected increase in the corresponding quadratic hyperpolarizability. The results showed that these complexes could be good candidates for SONLO switches acting through a redox mechanism because an 8.3-fold increase in the quadratic hyperpolarizability was predicted upon oxidation.

In this work we report the synthesis of a series of η^5-monocyclopentadienyliron(II)/ruthenium(II) complexes of the general formula $[M(\eta^5\text{-}C_5H_5)(PP)(L)][PF_6]$ {M = Fe, PP = dppe; M = Ru, PP = dppe or $2PPh_3$, L = 5-[3-(thiophen-2-yl)benzo[*c*]thiophenyl]thiophene-2-carbonitrile} to evaluate their molecular quadratic hyperpolarizabilities. Attempts to obtain the oxidized M^{III} complexes to study the corresponding quadratic hyperpolarizabilities for their potential use as SONLO switches operating by a redox mechanism were unsuccessful due to the low stability of the oxidized species. The quadratic hyperpolarizabilities were measured by hyper-Rayleigh scattering (HRS) at the fundamental wavelength of 1500 nm. DFT calculations were performed to gain an understanding of the second-order NLO mechanism in the titled complexes in solvated media with the objective of obtaining quantitatively satisfactory results for both the calculated electronic excitations and the quadratic hyperpolarizabilities in comparison with experimental data.

Results and Discussion

Synthesis and Spectroscopic Studies

The procedure used for the synthesis of the ligand 5-[3-(thiophen-2-yl)benzo[*c*]thiophenyl]thiophene-2-carbonitrile (**L1**) is depicted in Scheme 1. The 1,3-di(thiophen-2-yl)-benzo[*c*]thiophene skeleton (**3**) was synthesized according to the method of Kiebooms et al.[35] in three steps. First, the reaction of phthaloyl dichloride with 2-mercaptopyridine gave the *S*-(2-pyridinyl) thioester compound (**2**), which was treated with the freshly prepared Grignard reagent thiophen-2-ylmagnesium bromide. The resulting 1,2-phenylenebis(thiophen-2-ylmethanone) (**3**) was treated with Lawesson's reagent to give the desired 1,3-di(thiophen-2-yl)-benzo[*c*]thiophene (**4**) in good yields. The 1,3-di(thiophen-2-yl)benzo[*c*]thiophene was further functionalized by the Wielsmeyer–Haack reaction to afford the corresponding aldehyde **5**. The reaction of **5** with hydroxylammonium chloride in pyridine followed by dehydration with acetic anhydride afforded **L1** in good yield. The ligand was fully characterized by FTIR and ^1H and ^{13}C NMR spectroscopy. The solid-state IR spectra (KBr pellets) showed the characteristic stretching vibration of the nitrile functional group at 2203 cm^{-1}.

Complexes of general formula $[M(\eta^5\text{-}C_5H_5)(PP)(L1)][PF_6]$ (M = Ru, PP = dppe, $2PPh_3$; M = Fe, PP = dppe) were prepared by halide abstraction with $TlPF_6$ from the parent neutral complexes $[M(\eta^5\text{-}C_5H_5)(PP)X]$ (M =

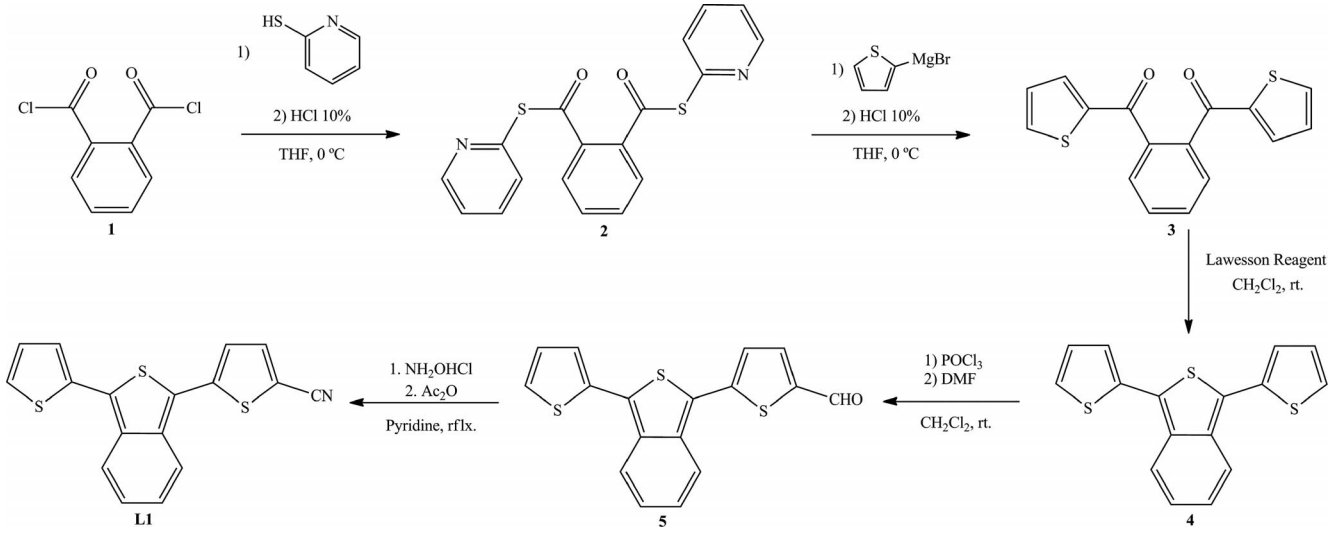

Scheme 1. Synthesis of the ligand **L1**.

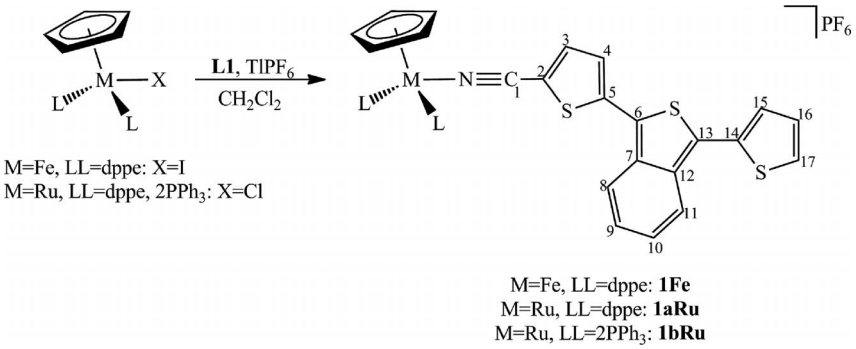

Scheme 2. Synthesis of benzo[*c*]thiophene-derived Ru/Fe complexes and the numbering scheme for the NMR spectral assignments.

Table 1. Selected IR and ^{1}H and ^{13}C NMR data for the Ru^{II}/Fe^{II} organometallic complexes.[a]

	ν(N≡C) [cm^{-1}]	δ_H [ppm]		δ_C [ppm]				
		3-H	4-H	C-1	C-2	C-3	C-4	C-5
1Fe	2196	6.88	7.30	128.38	108.01	139.81	125.38	143.47
	(–7)	(–1.05)	(–0.30)	(13.82)	(–0.48)	(–0.12)	(–1.06)	(0.13)
1aRu	2211	6.93	7.33	131.48	107.16	140.25	125.52	144.29
	(+8)	(–1.00)	(–0.27)	(16.92)	(–1.33)	(0.32)	(–0.92)	(0.95)
1bRu	2213	7.67	7.56	125.68	107.47	141.09	125.99	144.78
	(+10)	(–0.26)	(–0.04)	(11.12)	(–1.02)	(1.16)	(–0.45)	(1.44)

[a] Differences in the IR ν(N≡C) ($\nu_{complex} - \nu_{ligand}$) and NMR ^{1}H and ^{13}C resonances ($\delta_{complex} - \delta_{ligand}$) of the ligand upon coordination to the organometallic fragments are shown in parentheses.

Fe^{II}, X = I; M = Ru^{II}, X = Cl) in dichloromethane at room temperature in the presence of a sufficient excess of the corresponding ligand (Scheme 2). The complexes are fairly stable towards oxidation in air and to moisture both in the solid state and in solution. The compounds were characterized by analytical data, FTIR and ^{1}H, ^{13}C and ^{31}P NMR spectroscopy, which supported the proposed formulations. Relevant spectroscopic data are presented in Table 1.

Characteristic IR bands confirm the presence of the cyclopentadienyl co-ligand (ca. 3000–3100 cm^{-1}), the PF_6^- counter anion (838 and 557 cm^{-1}) and the coordinated nitrile (2196–2213 cm^{-1}) in all the complexes. Comparison of ν(N≡C) upon coordination of the ligand reveals a negative shift of 7 cm^{-1} for **1**Fe and a positive shift of 8 and 10 cm^{-1} for **1**aRu and **1**bRu, respectively. The negative shift can be attributed to the enhancement of the π-back-donation from the metal d orbitals to the π* orbital of the NC group, which leads to a decrease in the bond order of N≡C. The magnitude of this π-back-donation is thus higher for the iron(II) compound, as expected considering the better π-donating ability of the iron(II) moiety. The benzo[*c*]thiophene derivatives described here show more effective π-back-donation than those possessing terthiophene units with an acceptor nitro end-group in related oligothiophene iron(II)[14] and ruthenium(II)[13] complexes. Moreover, less effective π-back-donation was found in comparison with parent 1,2-di(2-thienyl)ethene iron(II) and ruthenium(II)[12] complexes, which possess one vinylidene unit between the two thiophene rings.

^{1}H NMR resonances for the cyclopentadienyl ring are in the range usually observed for monocationic ruthenium(II) and iron(II) complexes. The effect of coordination of the nitrile ligand is mainly observed at the 3-H and 4-H protons (see Scheme 2 for numbering), the resonances of which are shifted upfield upon coordination to the organometallic moieties. The higher shielding effect observed for **1**Fe is consistent with the higher degree of π-back-donation for this compound deduced from the FTIR data. The substitution of the dppe co-ligand by $2PPh_3$ in the ruthenium complex results in reduced shielding of the 3-H and 4-H protons upon coordination. The ^{13}C NMR spectroscopic data confirm the trends found in the ^{1}H NMR spectra. The major changes in the ligand carbon resonances upon coordination were observed in the thienyl-nitrile moiety (carbons C-1 to C-5), in agreement with the behaviour observed in the ^{1}H NMR spectra. In particular, significant deshielding of the NC carbon (C-1) of the ligand was observed upon coordination, as expected. The ^{31}P NMR spectra show a single sharp signal for the phosphane co-ligands, which were deshielded upon coordination, as expected, in accord with the σ-donor character of these ligands. The resonances are in the range usually observed for monocationic ruthenium(II) and iron(II) complexes. The same general behaviour of the NMR resonances has been observed previously in related oligothiophene iron(II)[14] and ruthenium(II),[13] and 1,2-di(2-thienyl)ethene iron(II) and ruthenium(II)[12] complexes.

The optical absorption spectra of the complexes at concentrations of 1.0×10^{-5} M were recorded in chloroform and DMF. The spectrum of **1**Fe exemplifies the behaviour of the compounds studied in this work (Figure 1) and the optical data are summarized in Table 2. Figure 1 also includes the spectrum of L**1** for comparison.

The spectrum of L**1** is characterized by one absorption band in the UV region and one strong and broad absorp-

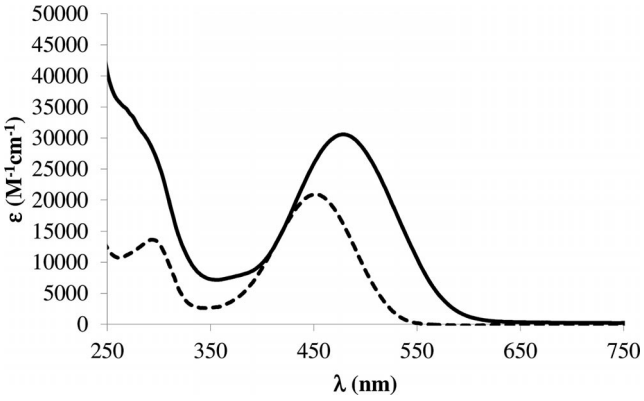

Figure 1. Electronic spectra of **1**Fe and the free ligand **L1** (dashed line) in chloroform.

Table 2. Optical spectral data for the synthesized complexes [M(η^5-C_5H_5)(PP)(L**1**)][PF_6] in chloroform and DMF.

	λ [nm] (ε [10^4 M^{-1}cm^{-1}]) $CHCl_3$	DMF	$\Delta\lambda$ [nm]
1Fe	478 (3.0) ≈290	464 (2.3) ≈291	–14
1aRu	475 (3.0) ≈280	473 (1.8) ≈288	–2
1bRu	473 (2.7) ≈280	453 (2.2) ≈291	–20

tion band in the visible region. The lowest-energy band is within the range found for benzo[*c*]thiophene derivatives[36,37] and can be assigned to a π–π* electronic transition. The main feature of the spectra of the complexes recorded in $CHCl_3$ is the presence of an intense broad band in the range of 473–478 nm with a band at higher energy (in the range of ca. 280–290 nm) depending on the organometallic fragment. To study the solvatochromic behaviour of the lowest-energy band, absorption spectra were also recorded in DMF. For all complexes a hypsochromic shift was observed upon increasing the solvent polarity, particularly for **1**Fe and **1**bRu (–14 and –20 nm, respectively). The negative solvatochromic behaviour exhibited by these compounds is characteristic of electronic transitions in which there is a decrease in the dipole moment upon excitation. A blueshift was also observed in the solvatochromic study of the ferrocenylethenyl-thienyl-2-thienylbenzo[*c*]thiophene organometallic complex.[33]

The energy and shape of the lowest-energy bands of the complexes resemble that of the uncoordinated ligand, which seems to indicate that they have high ILCT character. According to our recent TD-DFT calculations on model iron and ruthenium complexes with the formula [M(η^5-C_5H_5)($H_2PCH_2CH_2PH_2$)(L**1**)]$^+$ (similar to **1**Fe and **1**aRu) in the gas phase,[34] this band can be assigned to charge transfer mainly within the ligand fragment (ILCT). However, it is well known that solvation interactions are, in some cases, critical for obtaining quantitatively satisfactory results of the calculated electronic excitations in comparison with experimental data. Thus, for a deeper knowledge of the relevant electronic transitions involved, which can be helpful for further discussions on our experimentally determined first hyperpolarizabilities, we performed theoretical studies on model complexes taking into account solvation effects. The polarizable continuum model (PCM) was used to simulate the interaction between the complexes with chloroform. Also, we extended the theoretical studies to the synthesized ruthenium complexes (**1**aRu and **1**bRu) to evaluate the use of model phosphanes to describe the behaviour found with real molecules. The ligand **L1** was also included in these studies to enable a comparison with the results found for Fe^{II}/Ru^{II} complexes. Figure 2 shows the structures and atom labelling of the complexes used in our calculations.

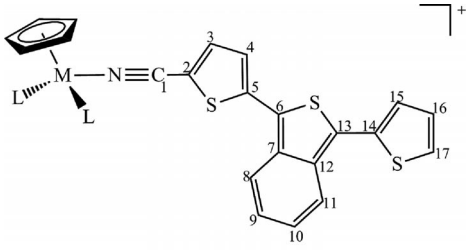

M=Fe, L,L= $H_2P(CH_2)_2PH_2$: **1'Fe**
M=Ru, L,L=$H_2P(CH_2)_2PH_2$: **1a'Ru**
M=Ru, L,L=dppe: **1aRu**
M=Ru, L=2PH_3: **1b'Ru**
M=Ru, L=2PPh_3: **1bRu**

Figure 2. Structures and atom labeling of the complexes used in the DFT calculations.

The optimized structures and selected structural data can be found in the Supporting Information. The angles and bond lengths are consistent with experimental crystal data

Table 3. Optical data for the studied compounds obtained by TD-DFT calculations in chloroform.

	λ_{eg}[a] [nm]	f[b]	Attribution[c]	Character of the CT[d]
L**1**	431 (452)	0.613	H→L (97%)	BcT (55), T2 (45)→NC-T1 (100)
1′Fe	447 (478)	0.852	H→L (93%)	BcT-T2 (93), Fe (4), Cp (3)→NC-T1 (96), P (4)
1a′Ru	486 (475)	0.964	H→L (96%)	BcT-T2 (92), Ru (4), Cp (4)→NC-T1 (96), P (4)
1b′Ru	477 (473)	0.936	H→L (96%)	BcT-T2 (95), Ru (5)→NC-T1 (100)
1aRu	465 (475)	0.952	H→L (96%)	BcT-T2 (90), Ru (5), P (5)→NC-T1 (100)
1bRu	475 (473)	1.008	H→L (96%)	BcT-T2 (75), Ru (19), Cp (6)→NC-T1 (100)

[a] Absorption wavelength of the main transitions (experimental values are shown in parentheses). [b] Oscillator strength. [c] H = HOMO, L = LUMO. [d] Based on the represented molecule fragments (overall % of the charge transfer is given in parentheses). Cp = cyclopentadienyl, NC = nitrile group, T = thiophene rings (T1 = thiophene close to NC; T2 = terminal thiophene), BcT = benzo[*c*]thiophene, P = phosphane co-ligands.

for the parent iron(II)[12] and ruthenium(II)[13] thiophene derivatives and other η^5-monocyclopentadienylmetal complexes.[15,38,39] After the geometry optimizations, the electronic spectra were simulated by means of TD-DFT calculations. Two bands are predicted, in accordance with our experimental spectra (a simulated spectrum for **1**′Fe is given in the Supporting Information). The results show that the lowest-energy band for all complexes, which is the key to second-order non-linear optical properties, arises mainly from a single electronic transition (HOMO→LUMO). The wavelengths, oscillator strengths and composition of this electronic transition in terms of the contributions of groups of atoms involved are given in Table 3.

Very good results for the calculated values of λ_{max} were obtained in comparison with the experimental data by using either model or real phosphanes in the calculations. In particular, the values of λ_{max} calculated for the ruthenium complexes (465 nm for **1**aRu and 475 nm for **1**bRu) are very close to the experimental values (475 and 473 nm, respectively). The analysis of the electronic transition in terms of the contributions of groups of atoms involved allowed us to predict reliable assignments of the band observed in the experimental spectra. The orbitals involved in the electronic transition are depicted in Figure 3. The results show that the character of this excitation resembles that of the free ligand, thus having mainly ILCT character. The corresponding electron density difference maps (EDDMs) clearly illustrate the transfer of the electron density from the terminal thiophene ring (T2) and benzo[*c*]thiophene group of the ligand to the NC-T1 moiety (Figure 4). However, there is also some contribution from MLCT. An enhanced contribution of the MLCT character is predicted when the real phosphanes dppe and PPh_3 were used in the calculations instead of $H_2P(CH_2)_2PH_2$ and PH_3. In particular, substitution of the model phosphane PH_3 (**1**b′Ru) by PPh_3 (**1**bRu) results in an increase in the contribution of the MLCT (from 5 to 25%) to the overall excitation.

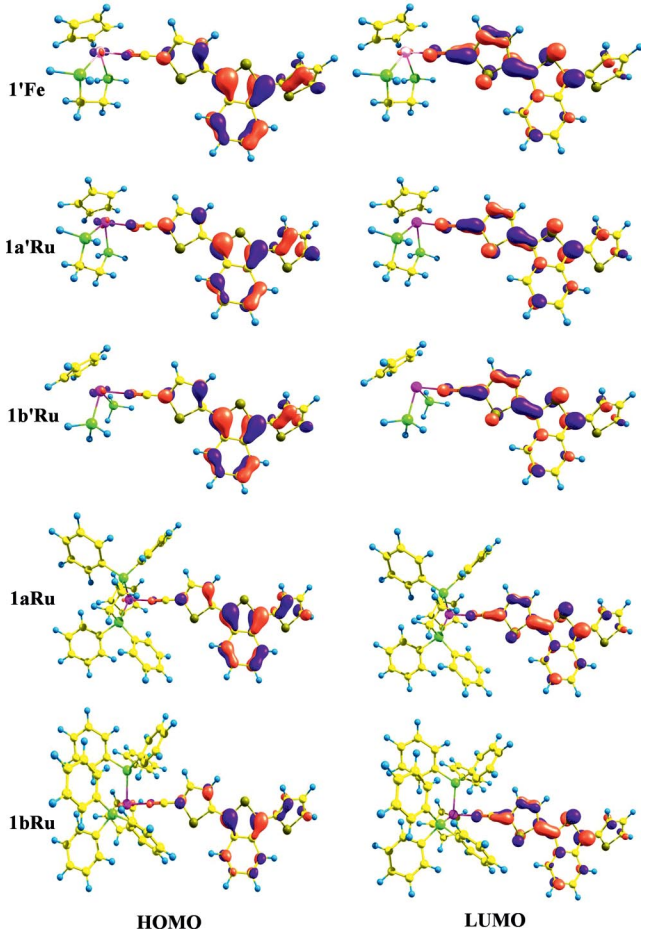

Figure 3. Representation of the main orbitals involved in the electronic transitions in the complexes **1**′Fe, **1**a′Ru, **1**b′Ru, **1**aRu and **1**bRu.

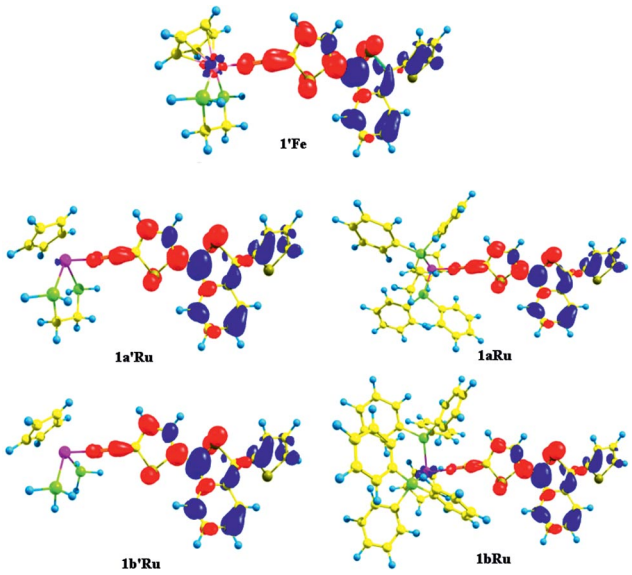

Figure 4. Electron density difference maps (EDDMs) of the HOMO–LUMO transition for the complexes **1**′Fe, **1**a′Ru, **1**b′Ru, **1**aRu and **1**bRu (red indicates an increase in electron density and blue indicates a decrease, isovalue = 0.002).

Electrochemical Studies

The redox behaviour of the compounds was studied by cyclic voltammetry in dichloromethane and acetonitrile, between the limits imposed by the solvents, to evaluate the electron richness at the active redox centres and the reversibility of the oxidation/reduction processes. The study of the reversibility of the redox processes gives an insight into the stability of the oxidized and/or reduced species. This is particularly important when dealing with NLO redox switching properties. In fact, to be used as molecular switches, both "on" and "off" forms must be stable and the switching process must be reversible. Thus, electrochemical studies are helpful to screen molecules with potential as molecular switches. As an example, the electrochemical response of **1**Fe in dichloromethane is shown in Figure 5 and the most important data exhibited by all the complexes and the free ligand in dichloromethane and acetonitrile are summarized in Table 4.

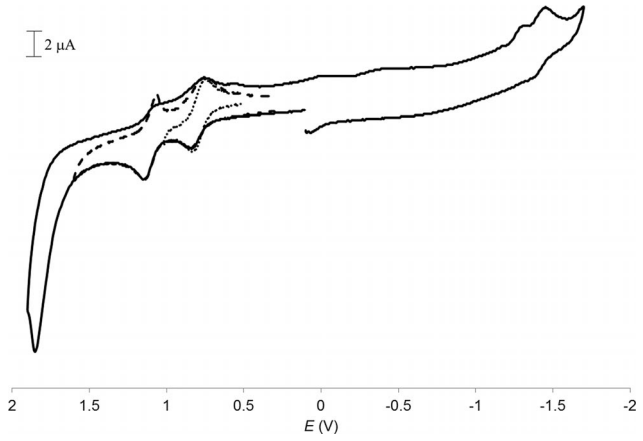

Figure 5. Cyclic voltammogram of complex **1**Fe in CH_2Cl_2 at 200 mV/s showing the reversibility of the isolated oxidative processes: (···) Fe^{II}/Fe^{III}, (---) both L1/L1^{ox} and Fe^{II}/Fe^{III}.

The electrochemistry of the free ligand L**1** is characterized by an irreversible oxidative process (E_{pa} = 1.00 V in dichloromethane, E_{pa} = 0.98 V acetonitrile) and two reductive processes at negative potentials. The reductive processes are irreversible in dichloromethane, but the first one becomes quasi-reversible in acetonitrile ($E_{1/2}$ = –1.36 V). Similar electrochemical behaviour was found for the related 5-(2-thiophen-2-ylvinyl)thiophene-2-carbonitrile[12] and 2,2′:5′,2′′-terthiophene-5-carbonitrile[40,41] compounds. The main electrochemical behaviour of the complexes is characterized by the presence of an oxidative process attributed to the M^{II}/M^{III} redox pair in addition to the processes at the positive and negative potentials already attributed to the coordinated ligand L**1**. The M^{II}/M^{III} redox process is reversible for the iron complex **1**Fe in both solvents ($E_{1/2}$ = 0.73 V in dichloromethane, $E_{1/2}$ = 0.68 V in acetonitrile). However, for the ruthenium complexes, this redox process was found to be irreversible (E_{pa} = 1.28 V for **1**aRu and E_{pa} = 1.29 V for **1**bRu in dichloromethane; E_{pa} ≈ 1.09 V for **1**aRu and E_{pa} = 1.23 V for **1**bRu in acetonitrile). The potential values of the ligand-related oxidative and reductive processes remained almost unchanged after coordination to the metal centres in both solvents. For the ruthenium complexes, all the processes are irreversible, and the same behaviour was found in dichloromethane for **1**Fe, but the first one becomes quasi-reversible in acetonitrile ($E_{1/2}$ = –1.38 V). In general, the organometallic complexes exhibit quite similar electrochemical behaviour to that observed for iron(II) and ruthenium(II) complexes bearing the related substituted thiophene-2-carbonitrile ligands.[12,13] In view of their potential use as second-order non-linear optical switches operating through redox mechanisms, and accord-

Table 4. Electrochemical data for complexes [M(η^5-C_5H_5)(PP)(L**1**)]PF_6] and free L**1** in CH_2Cl_2 and MeCN.

	E_{pa} [V]	E_{pc} [V]	$E_{1/2}$ [V]	$E_{pa} - E_{pc}$ [mV]	i_{pc}/i_{pa}
Dichloromethane					
L**1**	1.00	–	–	–	–
	–	–1.38	–	–	–
	–	–1.53	–	–	–
[Fe(η^5-C_5H_5)(dppe)(L**1**)][PF_6] (**1**Fe)	1.07	0.99	1.03	80	0.9
	0.77	0.68	0.73	90	0.9
	–	–1.37	–	–	–
	–	–1.53	–	–	–
[Ru(η^5-C_5H_5)(dppe)(L**1**)][PF_6] (**1**aRu)	1.28	–	–	–	–
	0.98	–	–	–	–
		–1.36			
		–1.53			
[Ru(η^5-C_5H_5)(PPh_3)$_2$(L**1**)][PF_6] (**1**bRu)	1.29	–	–	–	–
	1.01	–	–	–	–
		–1.38	–	–	–
		–1.55	–	–	–
Acetonitrile					
L**1**	1.13	–	–	–	–
	0.98	0.89	–	–	0.4
	–1.32	–1.39	–1.36	70	0.8[a]
		–1.71			
[Fe(η^5-C_5H_5)(dppe)(L**1**)][PF_6] (**1**Fe)	1.17	–	–	–	–
	1.09	–	–	–	–
	0.72	0.64	0.68	90	1.0
	–1.34	–1.42	–1.38	80	0.7[a]
		–1.72			
[Ru(η^5-C_5H_5)(dppe)(L**1**)][PF_6] (**1**aRu)	1.09[b]	–			
	–	–1.38			
	–	–1.70			
[Ru(η^5-C_5H_5)(PPh_3)2(L**1**)][PF_6] (**1**bRu)	1.23	–	–	–	–
	1.10	–	–	–	–
	0.97	–	–	–	–
		–1.39			
		–1.70			

[a] i_{pc}/i_{pa} values. [b] Very broad wave that incorporates three oxidative processes.

ing to the electrochemical behaviour of the complexes, it seems that only the iron complex may be suitable for this purpose owing to the reversibility of the Fe^{II}/Fe^{III} couple. However, attempts to synthesize and isolate the oxidized Fe^{III} complex have so far been unsuccessful due to its low stability. Further studies seeking to modify the molecular structure to obtain stable oxidized forms are currently in progress. Because it was not possible to achieve the oxidized M^{III} forms of the complexes, it will not be possible to evaluate the molecular switching based on the second-order NLO properties by redox means. Thus, only the quadratic hyperpolarizabilities of the M^{II} complexes were studied.

Quadratic Hyperpolarizabilities

Because the complexes exhibit optical transitions in the visible range, close to the second harmonic at 532 nm, high-resonance enhancements could be expected for β measurements at 1064 nm on the basis of the two-level model (TLM) of Oudar and Chemla.[42] Thus, experimental molecular quadratic hyperpolarizabilities (β) were measured by hyper-Rayleigh scattering (HRS) at 1500 nm to avoid the superposition of absorptions in the UV/Vis region and the second-harmonic signal (750 nm), where more reasonable results can be expected from the TLM analysis. The static hyperpolarizabilities of **1**aRu, **1**bRu and the model complexes **1**′Fe, **1**a′Ru and **1**b′Ru were computed by using DFT calculations to give an insight into the applicability of the TLM to the rationalization of the experimental NLO properties of the complexes studied. The results obtained are summarized in Table 5 together with relevant spectroscopic data.

Table 5. Quadratic hyperpolarizabilities and relevant spectroscopic data for the complexes $[M(\eta^5\text{-}C_5H_5)(PP)(L\mathbf{1})][PF_6]$.[a]

	$\Delta\nu_{(NC)}$[b] [cm^{-1}]	λ_{exp} [nm] (ε [10^4 M^{-1} cm^{-1}])	β_{HRS} [10^{-30} esu] Exp.	TLM[c]	DFT[d]
1Fe	–7	478 (3.0)	164	87	20.06[e]
1aRu	+8	475 (3.0)	147	80	24.73 24.72[f]
1bRu	+10	473 (2.7)	105	57	26.36 29.43[g]

[a] All measurements were performed in $CHCl_3$ solution. The β values were measured at 1500 nm (experimental error: 15%). [b] Differences in the IR ν(N≡C) band upon ligand coordination: $\nu_{complex}-\nu_{ligand}$. [c] β corrected for resonance enhancement by using the two-level model with $\beta_{TLM} = \beta_{exp}[1-(2\lambda_{max}/\lambda_{HRS})/2][1-(\lambda_{max}/\lambda_{HRS})/2]$ (damping factors not included). [d] β_{HRS} calculated by DFT using Equations (3)–(5) (the orientational averages and β tensor components are shown in the Supporting Information). The B convention[43] was used for direct comparison with experimental data. [e] Model complex **1**′Fe. [f] Model complex **1**a′Ru. [g] Model complex **1**b′Ru.

It is well known that the two-level model (TLM) is a good approximation for estimating quadratic hyperpolarizabilities in cases in which only one excited state is coupled strongly enough to the ground state by the applied electric field, and only one component of the β tensor dominates the NLO response (i.e., a unidirectional charge-transfer transition). This model establishes a link between the molecular hyperpolarizability and a low-lying energy charge-transfer transition expressed by Equation (1)

$$\beta \propto \frac{\Delta\mu_{eg} f_{eg}}{E_{eg}^3} \quad (1)$$

in which $\Delta\mu_{eg}$ is the difference between the dipole moments of the ground (g) and excited (e) states, f_{eg} is the oscillator strength and E_{eg} is the transition energy. An optimal combination of these factors will provide higher β values. The DFT calculations of the molecular hyperpolarizabilities show that all complexes are dominated by the β_{zzz} tensor component (along the charge-transfer axis) with a depolarization ratio (ρ) of around 1:5 [see Eq. (6) in the Exp. Sect. and the Supporting Information), which is expected for a prototypical 1D dipolar molecule.[44] In addition, TD-DFT calculations predicted a single dominant electronic transition in the visible region (HOMO→LUMO) for these complexes (Table 3). Thus, an analysis of the results according to the TLM seems to be reasonable for these complexes.

The experimental quadratic hyperpolarizabilities are relatively low, as expected considering the molecular nature of these complexes, which can be viewed as having a structure of the type D–π–D′ in which the well-known electron-donating character of the organometallic fragments is combined with the thiophene-benzo[*c*]thiophene moiety that behaves mainly as a donor during the lowest-energy transition (see above). The results show some resonant enhancement, although the relative orderings were maintained with the TLM corrected values: **1**Fe > **1**aRu > **1**bRu. In spite of the relatively similar magnitudes of the experimental quadratic hyperpolarizabilities for all the complexes (the values for **1**Fe and **1**aRu are within the experimental error), it is interesting to note that experimental quadratic hyperpolarizabilities follow the same trend as observed for the relative π-back-donation of the complexes deduced from the FTIR and NMR spectroscopic data. The existence of this interaction was found to play an important role in the second-order NLO response of the η^5-monocyclopentadienyliron, -ruthenium, -nickel and -cobalt complexes with *para*-substituted benzonitrile chromophores, with the high values found for the Ru^{II} and Fe^{II} complexes being attributed to π-back-donation.[18] The fact that the experimental quadratic hyperpolarizabilities for all the complexes are relatively similar is not surprising considering the spectroscopic data discussed above. In fact, for the low-energy band, which is the key to second-order non-linear optical properties, λ_{max} is very similar for all the complexes and no significant solvatochromic effect was observed. In addition, charge transfer was predicted by theoretical calculations to be of the same nature, mainly within the ligand (ILCT) with some MLCT contribution (see above). The use of dppe and PPh_3 instead of the models $H_2P(CH_2)_2PH_2$ and PH_3 in the DFT calculations, however, can give an additional insight into the differ-

ences in the experimental quadratic hyperpolarizabilities of the ruthenium complexes. As discussed above, DFT calculations on **1**bRu predicted an enhanced contribution of the MLCT to the overall excitation (ca. 25%). For **1**aRu, the contribution of the MLCT is lower (ca. 10%). The ILCT arises from charge transfer from the terminal thienyl ring and the benzo[*c*]thiophene moiety to the thienyl-nitrile unit whereas the MLCT occurs from the organometallic moiety also to the thienyl-nitrile unit. Thus, ILCT and MLCT have opposite directions of charge transfer. This might result in a lower charge-transfer efficiency during the electronic excitation for **1**bRu (which has a large MLCT contribution) and an expected lowering effect on the experimental quadratic hyperpolarizability.

DFT calculations predicted low β_{HRS} values for the model complexes, in the range of $(20.06–29.43) \times 10^{-30}$ esu. The substitution of the model phosphanes by dppe and PPh_3 originates small differences (up to ca. 10%) in the corresponding calculated β_{HRS}. The results show some underestimation of the DFT-calculated β_{HRS} values when compared with the experimental two-level model corrected values for **1**Fe, **1**aRu and **1**bRu. Different reasons for these discrepancies can be conjectured. For example, the use of averaged configurations of the complexes for the calculations instead of the minimum energy alone and the inclusion of solvated media with a more detailed model than PCM could probably lead to more realistic results. These issues have been discussed, for example, by Jensen and van Duijnen for the case of the widely studied *p*-nitroaniline[45] and further studies will be carried out taking them into account.

Conclusions

η^5-Monocyclopentadienyliron(II)/ruthenium(II) complexes bearing the 5-[3-(thiophen-2-yl)benzo[*c*]thiophenyl]-thiophene-2-carbonitrile ligand have been synthesized and fully characterized. Quadratic hyperpolarizabilities were determined by HRS measurements at 1500 nm, showing resonant values in the range $(105–164) \times 10^{-30}$ esu and corrected values, by application of the two-level-model, in the range $(57–87) \times 10^{-30}$ esu. Time-dependent density functional theory calculations were employed to gain a deeper knowledge of the relevant electronic transitions involved, which was very helpful in the discussion on the experimental quadratic hyperpolarizabilities. These properties were also computed by using DFT. These results, together with TD-DFT data, showed that TLM could be used to rationalize the experimentally observed NLO properties of the studied complexes. The observed quadratic hyperpolarizabilities, similar for all complexes, can be explained by the very similar energies and intensities of the lowest-energy electronic transition, which are shown to have mainly ILCT character. The use of real and model phosphanes to simulate the electronic spectra of the complexes by DFT calculations shows no significant differences between the calculated energies and the experimental data. Therefore the use of model phosphanes, with the obvious gain in computational cost, proves to be a good compromise between the accuracy of the predicted excitation energies and computational effort. However, the results show that the use of real phosphanes in DFT calculations can be important to provide an additional understanding of the experimental values of the quadratic hyperpolarizabilities. In comparison with the experimental TLM corrected data, DFT calculations underestimate to some extent the β_{HRS} values of the studied complexes.

Experimental Section

General Procedures: Syntheses were carried out under nitrogen by using current Schlenk techniques and the solvents were dried by standard methods.[46] Commercial reagents were used without further purification. Organometallic starting materials were prepared following methods described in the literature: [Fe(η^5-C_5H_5)(dppe)I],[14] [Ru(η^5-C_5H_5)(PPh_3)$_2$Cl] and [Ru(η^5-C_5H_5)(dppe)Cl].[47] Compounds **1**–**3** were prepared following published procedures[35] with some modifications (see details below). 5-(3-Thiophen-2-yl-benzo[*c*]thiophenyl)thiophene-2-carbaldehyde (**5**) was prepared following a published procedure[48] but with a different purification method (see details below). FTIR spectra were recorded with a Mattson Satellite FTIR spectrophotometer in dry KBr pellets (only significant bands are cited). ^{1}H, ^{13}C and ^{31}P NMR spectra were recorded with a Bruker Avance 400 spectrometer at probe temperature using $CDCl_3$ or $(CD_3)_2CO$ as solvent. The ^{1}H and ^{13}C chemical shifts are reported in parts per million (ppm) downfield from internal Me_4Si and the ^{31}P chemical shifts are reported in ppm downfield from 85% H_3PO_4 as external standard. Coupling constants are reported in Hz and spectral assignments follow the numbering scheme shown in Scheme 2 and were assigned by using HMBC, HMQC and/or COSY NMR techniques. UV/Vis spectra were recorded with a Jasco V-560 spectrophotometer in the range of 200–900 nm in dried solvents. Elemental analyses were obtained at our laboratories (Laboratório de Análises, Instituto Superior Técnico) by using a Fisons Instruments EA1108 system. Data acquisition, integration and handling were performed by using a PC with the EAGER-200 software package (Carlo–Erba Instruments).

Synthesis

***S*,*S*-Di(pyridin-2-yl)benzene-1,2-bis(carbothioate) (2):** Triethylamine (5 mL) and 2-mercaptopyridine (3.3 g, 30 mmol) were added to dried thf (50 mL). After stirring for 10 min, full dissolution of the 2-mercaptopyridine was observed, the mixture was placed in an ice-cold bath and stirred at 0 °C for a further 15 min. A solution of phthaloyl chloride (2.2 mL, 15 mmol) in dried thf (50 mL) was added in one portion and with vigorous stirring. The reaction was quenched immediately with 2% aq. HCl solution (200 mL) and extracted with chloroform. The combined organic fractions were washed with 10% aq. NaOH and water until neutral, dried with anhydrous $MgSO_4$ and the solvent was evaporated in vacuo. Crystallization from $CHCl_3$/diethyl ether afforded the desired product as white needles in 80% yield. ^{1}H NMR (400 MHz, $CDCl_3$, 25 °C): δ = 7.24 (dt, 2 H, H_{py}), 7.59 (m, 2 H, H_{benz}), 7.71 (m, 4 H, H_{py}), 7.82 (m, 2 H, H_{benz}), 8.57 (d, 2 H, H_{py}) ppm.

1,2-Phenylenebis(thiophen-2-ylmethanone) (3): 2-Bromothiophene (4.5 mL, 46 mmol) was added to a Schlenk flask with thf (100 mL) containing activated magnesium turnings (1.2 g, 46 mmol) and a

catalytic amount of iodine. The mixture was heated at a gentle reflux for 3 h until complete reaction of the magnesium and then left to cool at room temperature. The Grignard solution was added dropwise through a Teflon cannula to a stirred solution of **2** (7.95 g, 23 mmol) in thf (150 mL) at 0 °C. The resulting mixture was stirred for an additional 30 min and quenched with 10% aq. HCl (200 mL) solution. After extraction with several portions of chloroform, the combined organic extracts were washed with 10% aq. NaOH, followed by aq. $NaHCO_3$, and finally water. After drying with anhydrous $MgSO_4$, the solvent was removed in vacuo. Crystallization from $CHCl_3$/petroleum ether (40–60) afforded a brownish orange solid in 90% yield. ^{1}H NMR [400 MHz, $(CD_3)_2CO$, 25 °C]: δ = 7.19 (dt, 2 H, H_{th}), 7.59 (dd, 2 H, H_{th}), 7.78 (m, 2 H, H_{benz}), 7.83 (m, 2 H, H_{benz}), 7.97 (dd, 2 H, H_{th}) ppm.

1,3-Di(thiophen-2-yl)benzo[*c*]thiophene (4): Lawesson's reagent (8.13 g, 20.1 mmol) was added in two portions to a solution of **3** (6.0 g, 20.1 mmol) in dichloromethane (100 mL). After stirring overnight, the solvent was removed under vacuum and ethanol (100 mL) was added. This solution was stirred with heating for 30 min. The solvent was removed and the brown residue was added to dichloromethane, washed with 10% aq. NaOH and several times with water. After drying with anhydrous $MgSO_4$ followed by filtration, the solvent was evaporated in vacuo and the resultant brownish orange solid was purified by chromatography on silica gel. Elution with petroleum ether (40–60) afforded the desired product as orange crystals in 55% yield. ^{1}H NMR (400 MHz, $(CD_3)_2CO$, 25 °C): δ = 7.26 (m, 2 H, H_{th}), 7.51 (dd, 2 H, H_{th}), 7.64 (dd, 2 H, H_{th}), 8.00 (m, 2 H, H_{benz}) ppm.

5-[3-(Thiophen-2-yl)benzo[*c*]thiophenyl]thiophene-2-carbaldehyde (5): A mixture of phosphorus oxychloride (2.42 mL, 26 mmol) and DMF (2 mL, 26 mmol) in dichloromethane (10 mL) was added to a solution of **4** (1.55 g, 5.2 mmol) in dichloromethane (50 mL) at room temperature. After stirring overnight, a saturated solution of sodium acetate (100 mL) was added and the mixture was stirred for 1 h to complete the hydrolysis. The suspension formed was extracted with dichloromethane. The combined organic layers were washed with water, dried with $MgSO_4$, and the solvent removed in vacuo. The red solid obtained was purified by chromatography on silica gel. Elution with petroleum ether (40–60)/diethyl ether (7:3 to 1:1) afforded the desired product as red crystals in 80% yield. ^{1}H NMR [400 MHz, $(CD_3)_2CO$, 25 °C]: δ = 7.26 (m, 2 H, 2-H), 7.51 (dd, 2 H, 3-H), 7.64 (dd, 2 H, 1-H), 8.00 (m, 2 H, 4-H, 5-H) ppm.

5-[3-(Thiophen-2-yl)benzo[*c*]thiophenyl]thiophene-2-carbonitrile (L1): A solution of $H_2NOHHCl$ (2.13 g, 30.7 mmol) in pyridine (10 mL) was added to a stirred solution of **5** (2.0 g, 6.13 mmol) in pyridine (30 mL) cooled to 0 °C. The reaction was allowed to warm to room temperature. After stirring for 1 h, acetic anhydride (5 mL) was added dropwise and the mixture was heated at reflux for 2 h. After cooling to room temperature, the mixture was poured into a mixture of ice and 10% aq. HCl. The resulting orange precipitate was dissolved in dichloromethane, washed with water and dried with $MgSO_4$. The solvent was removed in vacuo and the crude product was purified by column chromatography on silica gel. Elution with a solvent gradient from petroleum ether (40–60)/diethyl ether, 7:3 to 1:1, afforded the desired product as an orange solid in 72% yield. IR (KBr): $\tilde{\nu}$ = 2203 (N≡C) cm^{-1}. ^{1}H NMR [400 MHz, $(CD_3)_2CO$, 25 °C]: δ = 7.27 (dt, 1 H, 16-H), 7.30 (dt, 1 H, 11-H), 7.37 (dt, 1 H, 8-H), 7.57 [dd, $^3J_{H,H}$ = 3.7, 1.0 Hz, 1 H, 17-H], 7.60 (d, $^3J_{H,H}$ = 4.1 Hz, 1 H, 4-H), 7.71 (dd, $^3J_{H,H}$ = 5.3, 1.0 Hz, 1 H, 15-H), 7.93 (d, $^3J_{H,H}$ = 4.1 Hz, 1 H, 3-H), 8.03 (t, $^3J_{H,H}$ = 9.0 Hz, 1 H, 9-H, 10-H) ppm. ^{13}C NMR [100 MHz, $(CD_3)_2CO$, 25 °C]: δ = 108.49 (C-2), 114.56 (C-1), 121.76 (C-10), 122.63 (C-9), 123.87 (C-6), 126.33 (C-11), 126.44 (C-4), 127.66 (C-17), 127.74 (C-8), 128.07 (C-15), 129.35 (C-16), 130.57 (C-13), 135.10 (C-14), 136.09 (C-12), 137.13 (C-7), 139.93 (C-3), 143.34 (C-5) ppm. UV/Vis ($CHCl_3$): λ_{max} (ε) = 452 nm (2.1×10^4 M^{-1} cm^{-1}). $C_{17}H_9NS_3 \cdot 0.1CH_2Cl_2$ (323.46): calcd. C 61.87, H 2.79, N 4.22, S 28.98; found C 61.81, H 3.01, N 3.96, S 27.75.

General Procedure for the Synthesis of the [M(η^5-C_5H_5)(LL)L1]PF_6 Complexes: The complexes were synthesized by halogen abstraction from the organometallic precursors in a Schlenk tube. A mixture of [M(η^5-C_5H_5)(LL)X] (0.5 mmol), $TlPF_6$ (1.5 equiv.) and **L1** (1.1 equiv.) in freshly dried dichloromethane (30 mL) was heated at reflux overnight under nitrogen. After filtration to remove the TlX formed during the reaction, the solvent was evaporated under vacuum and the solid residues were recrystallized twice from dichloromethane/hexane to afford the desired compounds as reddish solids.

[Fe(η^5-C_5H_5)(dppe)L1]PF_6 (1Fe): Dark red, yield 360 mg, 73%. IR (KBr): $\tilde{\nu}$ = 2196 (N≡C), 838 and 557 (PF_6^-) cm^{-1}. ^{1}H NMR [400 MHz, $(CD_3)_2CO$, 25 °C]: δ = 2.67 (m, 2 H, CH_2), 2.84 (m, 2 H, CH_2), 4.71 (s, 5 H, η^5-C_5H_5), 6.88 (d, $^3J_{H,H}$ = 4.1 Hz, 1 H, 3-H), 7.28 (dt, 1 H, 16-H), 7.30 (d, $^3J_{H,H}$ = 4.1 Hz, 1 H, 4-H), 7.34 (dt, 1 H, 8-H), 7.43 (dt, 1 H, 11-H), 7.55 (dt, 1 H, 17-H), 7.57 (m, 8 H, $H_{o\text{-}Ph}$), 7.68 (m, 8 H, $H_{m\text{-}Ph}$), 7.71 (dt, 1 H, 15-H), 7.81 (d, $^3J_{H,H}$ = 8.9 Hz, 1 H, 10-H), 8.04 (d, $^3J_{H,H}$ = 8.9 Hz, 1 H, 9-H), 8.12 (m, 4 H, $H_{p\text{-}Ph}$) ppm. ^{13}C NMR [100 MHz, $(CD_3)_2CO$, 25 °C]: δ = 28.51 (t, $^1J_{C,P}$ = 42.0 Hz, CH_2-dppe), 81.12 (η^5-C_5H_5), 108.01 (C-2), 121.56 (C-10), 122.83 (C-9), 123.77 (C-6), 125.38 (C-4), 126.52 (C-11), 127.89 (C-15), 127.92 (C-8), 128.31 (C-17), 128.38 (C-1), 129.43 (C-16), 130.06 and 130.27 (t, $J_{C,P}$ = 10.0 Hz, $C_{m\text{-}Ph}$), 131.04 (C-13), 131.41 and 131.85 (s, $C_{p\text{-}Ph}$), 132.41 and 134.03 (t, $J_{C,P}$ = 10.0 Hz, $C_{o\text{-}Ph}$), 134.92 (C-14), 136.07 (C-12), 137.03 (C-7), 137.61 (t, $J_{C,P}$ = 41.0 Hz, $C_{i\text{-}Ph}$), 139.81 (C-3), 143.47 (C-5) ppm. ^{31}P NMR [161 MHz, $(CD_3)_2CO$, 25 °C]: δ = 96.98 (s, dppe), –144.25 (sept, PF_6^-) ppm. UV/Vis. ($CHCl_3$): λ_{max} (ε) = 478 nm (3.0×10^4 M^{-1} cm^{-1}). $C_{48}H_{38}F_6FeNP_3S_3 \cdot 1/3CH_2Cl_2$ (987.77): calcd. C 57.13, H 3.84, N 1.38, S 9.47; found C 57.25, H 3.66, N 1.42, S 9.34.

[Ru(η^5-C_5H_5)(dppe)L1]PF_6 (1aRu): Light red, yield 284 mg, 55% yield. IR (KBr): $\tilde{\nu}$ = 2211 (N≡C), 838 and 557 (PF_6^-) cm^{-1}. ^{1}H NMR (400 MHz, $(CD_3)_2CO$, 25 °C): δ = 1.89 (m, 2 H, CH_2), 2.20 (m, 2 H, CH_2), 5.06 (s, 5 H, η^5-C_5H_5), 6.93 (d, $^3J_{H,H}$ = 4.0 Hz, 1 H, 3-H), 7.28 (dt, 1 H, 16-H), 7.33 (d, $^3J_{H,H}$ = 4.0 Hz, 1 H, 4-H), 7.43 (dt, 1 H, 8-H), 7.50 (1 H, 11-H), 7.53 (m, 8 H, $H_{o\text{-}Ph}$), 7.56 (dt, 1 H, 17-H), 7.66 (m, 8 H, $H_{m\text{-}Ph}$), 7.73 (dt, 1 H, 15-H), 7.83 (d, $^3J_{H,H}$ = 8.0 Hz, 1 H, 10-H), 8.05 (1 H, 9-H), 8.06 (m, 8 H, $H_{p\text{-}Ph}$) ppm. ^{13}C NMR [100 MHz, $(CD_3)_2CO$, 25 °C]: δ = 28.53 (t, $^1J_{C,P}$ = 46 Hz, CH_2-dppe), 83.53 (η^5-C_5H_5), 107.16 (C-2), 121.54 (C-10), 122.86 (C-9), 123.63 (C-6), 125.52 (C-4), 126.54 (C-11), 127.95 (C-15), 128.01 (C-8), 128.38 (C-17), 129.45 (C-16), 129.88 and 130.11 (t, $J_{C,P}$ = 9.00 Hz, $C_{m\text{-}Ph}$), 131.30 and 131.80 (s, $C_{p\text{-}Ph}$), 131.48 (C-1), 131.98 and 134.28 (t, $J_{C,P}$ = 22.0 Hz, $C_{o\text{-}Ph}$), 134.90 (C-14), 136.10 (C-12), 137.12 (C-7), 140.25 (C-3), 144.29 (C-5) ppm ppm. ^{31}P NMR [161 MHz, $(CD_3)_2CO$, 25 °C]: δ = 79.07 (s, dppe), –144.26 (sept, PF_6^-) ppm. UV/Vis. ($CHCl_3$): λ_{max} (ε) = 475 (3.0×10^4 M^{-1} cm^{-1}). $C_{48}H_{38}F_6NP_3RuS_3 \cdot 2CH_2Cl_2$ (1033.00): calcd. C 49.93, H 3.52, N 1.16, S 8.00; found C 50.40, H 3.60, N 1.20, S 8.00.

[Ru(η^5-C_5H_5)(PPh_3)$_2$L1]PF_6 (1bRu): Dark red, yield 361 mg, 62%. IR (KBr): $\tilde{\nu}$ = 2213 (N≡C), 838 and 557 (PF_6^-) cm^{-1}. ^{1}H NMR [400 MHz, $(CD_3)_2CO$, 25 °C]: δ = 4.79 (s, 5 H, η^5-C_5H_5), 7.27 (m, 12 H, $H_{o\text{-}Ph}$), 7.29 (1 H, 16-H), 7.34 (dt, 1 H, 8-H), 7.39 (m, 12 H,

$H_{m\text{-Ph}}$), 7.44 (dt, 1 H, 11-H), 7.49 (m, 6 H, $H_{p\text{-Ph}}$), 7.56 (d, $^3J_{H,H}$ = 4.1 Hz, 1 H, 4-H), 7.59 (dd, $^3J_{H,H}$ = 4.0, 0.9 Hz, 1 H, 17-H), 7.67 (d, $^3J_{H,H}$ = 4.1 Hz, 1 H, 3-H), 7.73 (dd, $^3J_{H,H}$ = 4.0, 0.9 Hz, 1 H, 15-H), 7.94 (d, $^3J_{H,H}$ = 8.0 Hz, 1 H, 10-H), 8.07 (d, $^3J_{H,H}$ = 8.0 Hz, 1 H, 9-H) ppm. ^{13}C NMR [100 MHz, $(CD_3)_2CO$, 25 °C]: δ = 85.31 (η^5-C_5H_5), 107.47 (C-2), 121.62 (C-10), 122.88 (C-9), 123.67 (C-6), 125.68 (C-1), 125.99 (C-4), 126.58 (C-11), 128.00 (C-15), 128.09 (C-17), 128.41 (C-8), 129.44 (t, *J*CP = 9.0 Hz, $C_{m\text{-Ph}}$), 131.14 (s, $C_{p\text{-Ph}}$), 131.49 (C-13), 134.29 (t, $J_{C,P}$ = 11.0 Hz, $C_{o\text{-Ph}}$), 134.91 (C-14), 136.13 (C-12), 136.48 (t, $J_{C,P}$ = 44.0 Hz, $C_{i\text{-Ph}}$), 137.27 (C-7), 141.09 (C-3), 144.78 (C-5) ppm. ^{31}P NMR [161 MHz, $(CD_3)_2CO$, 25 °C]: δ = 41.35 (s, dppe), –144.27 (sept, PF_6^-) ppm. UV/Vis ($CHCl_3$): λ_{max} (ε) = 473 (2.7×10^4 M^{-1} cm^{-1}). $C_{58}H_{44}F_6NP_3RuS_3\cdot 1/4CH_2Cl_2$ (1159.15): calcd. C 59.27, H 3.80, N 1.19, S 8.15; found C 59.27, H 4.12, N 1.19, S 7.82.

Electrochemical Studies: Electrochemical experiments were performed with an EG&G Princeton Applied Research Potentiostat/Galvanostat Model 273A instrument equipped with Electrochemical PowerSuite v2.51 software for electrochemical analysis. Cyclic voltammograms were recorded in CH_2Cl_2 and CH_3CN with $[Bu_4N][PF_6]$ (0.1 M) as the supporting electrolyte. The electrochemical cell was a three-electrode configuration cell with a platinum disc working electrode (1.0 mm) probed by a Luggin capillary connected to a silver wire pseudo-reference electrode and a platinum wire auxiliary electrode. All the experiments were performed under argon at room temperature. All the reported potentials were measured against the ferrocene/ferrocenium redox couple as internal standard and are normally quoted relative to SCE (using the ferrocenium/ferrocene redox couple $E_{1/2}$ = 0.46 or 0.40 V vs. SCE for dichloromethane or acetonitrile, respectively[49]). The electrochemical-grade electrolyte was purchased from Aldrich Chemical Co. and dried under vacuum at 110 °C for 24 h. Reagent-grade solvents were dried, purified by standard procedures,[46] and distilled under nitrogen before use.

HRS Measurements of the First Hyperpolarizabilities: The first hyperpolarizabilities (β) were measured by using the harmonic light scattering technique (also named hyper-Rayleigh) in chloroform. The 10^{-3}–10^{-5} M solutions of the complexes were placed in a 4 cm long fluorimetric cell after being carefully filtered through a 0.2 mm filter to eliminate the white light noise resulting from microburning any of the remaining dust particles by the incoming laser beam. The measurements were performed at a fundamental wavelength of 1500 nm as described by Stadler et al.[50] using a Q-switched Nd:YAG laser operating in the 10 Hz repetition range. The scattered second harmonic signal was collected at 90° with respect to the direction of the incoming laser beam. The molecular hyperpolarizabilities were derived from the HRS data by using the external reference method. Disperse red 1 (DR1) dissolved in chloroform was used as the external standard. The reference hyperpolarizability (β) of DR1 in $CHCl_3$ was measured by comparison of the slopes of I_{2w} vs. the concentration plot of the standard in CH_2Cl_2 and $CHCl_3$.[44] By using the hyperpolarizability of DR1 in dichloromethane [β_{DR1} (CH_2Cl_2) = 70×10^{-30} esu],[51] the hyperpolarizability of DR1 in $CHCl_3$ was estimated to be 80×10^{-30} esu, which is very close to the published value of 74×10^{-30} esu.[50] The effect of the refractive indices of the solvents was corrected by using a simple Lorentzian local field.[52] Assuming that the scattering contribution from the solvent is negligibly small, this external reference method was then used to calculate the β_{HRS} values of complexes according to Equation (2)[44] in which $\langle\beta_{HRS}^2\rangle$ is the orientational average of the β tensor and S is the slope of the appropriate "I_{2w} versus concentration" plot (the subscripts c and ref refer to the complexes and reference sample, respectively). For the classic 90° angle geometry HRS experiment and for an unpolarized scattered signal, the orientational average over β is given by Equation (3).[44]

$$\left\langle\beta_{HRS}^2\right\rangle_c = \frac{S_c}{S_{ref}}\left\langle\beta_{HRS}^2\right\rangle_{ref} \tag{2}$$

$$\left\langle\beta_{HRS}^2\right\rangle = \left\langle\beta_{ZZZ}^2\right\rangle + \left\langle\beta_{XZZ}^2\right\rangle \tag{3}$$

The macroscopic averages in Equation (3) can be written as a function of the β-tensor components in the molecular frame (without assuming Kleinman's symmetry conditions) according to the method developed by Bersohn et al.[53] For transparent and weak optically dispersive materials, the Kleinman symmetry conditions[54] can be applied to the β-tensor components. Thus, the orientational averages involved in Equation (3) can be simplified to Equations (4) and (5).[55]

$$\left\langle\beta_{ZZZ}^2\right\rangle = \frac{1}{7}\sum_i^{x,y,z}\beta_{iii}^2 + \frac{6}{35}\sum_{i\neq j}^{x,y,z}\beta_{iii}\beta_{ijj} + \frac{9}{35}\sum_{i\neq j}^{x,y,z}\beta_{ijj}^2 + \frac{6}{35}\sum_{ijk,cyclic}^{x,y,z}\beta_{ijj}\beta_{jkk} + \frac{12}{35}\beta_{ijk}^2 \tag{4}$$

$$\left\langle\beta_{XZZ}^2\right\rangle = \frac{1}{35}\sum_i^{x,y,z}\beta_{iii}^2 - \frac{2}{105}\sum_{i\neq j}^{x,y,z}\beta_{iii}\beta_{ijj} + \frac{11}{105}\sum_{i\neq j}^{x,y,z}\beta_{ijj}^2 - \frac{2}{105}\sum_{ijk,cyclic}^{x,y,z}\beta_{ijj}\beta_{jkk} + \frac{8}{35}\beta_{ijk}^2 \tag{5}$$

The associated depolarization ratio (ρ) is defined by Equation (6).

$$\rho = \frac{\left\langle\beta_{XZZ}^2\right\rangle}{\left\langle\beta_{ZZZ}^2\right\rangle} \tag{6}$$

As an example, for a prototypical one-dimensional extended dipolar molecule with the single major diagonal tensor component β_{zzz}, the depolarization ratio is 1:5.[44]

DFT Calculations: All calculations were performed at the DFT level of theory by using the Gaussian 09 package.[56] The solvation effects were simulated by using the polarizable continuum model (PCM) as implemented in Gaussian 09. The hybrid functional CAM-B3LYP[57] (Coulomb-Attenuating Method applied to B3LYP) was used for the calculations. As a compromise between accuracy and computational effort we adopted the 6–31G* (for geometry optimizations) and the 6–31+G* basis sets (for calculation of the hyperpolarizabilities) for C, H, N, O and H, and the LANL2DZ effective core potential basis set for S, P, Fe and Ru.[58,59] In the case of the calculations of the hyperpolarizabilities, the LANL2DZ basis set was also augmented with a polarization function (exponents of 0.496 and 0.364) and a diffuse function (exponents of 0.0347 and 0.0298) for elements S and P, respectively.[60–62] Geometry optimizations were performed without any symmetry constraints. In all cases, the Hessian was computed to confirm the stationary points of the potential energy surfaces (PES) as true minima. The static first hyperpolarizability tensor components (β_{ijk}), for all compounds were calculated by means of the analytic gradient methodology adopted in the Gaussian 09 program package. These terms were used to calculate β_{HRS} according to Equation (3), after the summations given by Equations (4) and

(5). The reported β_{ijk} tensor components (presented in the Supporting Information) are in accord with the Taylor series expansion (T convention). To compare with experimental HRS values, which follows the power series expansion of the dipole moment as a function of the external fields (B convention), the calculated β_{HRS} presented in Table 5 were previously converted into the B convention. The relation between the hyperpolarizabilities in these conventions is $1/2\beta^T = \beta^B$.[43] TD-DFT[63,64] was used to compute the electronic spectra of the studied molecules applying the same level of theory and basis sets as used for the calculation of the hyperpolarizabilities. The first 24 lowest excitation energies were computed and the simulated absorption bands were obtained by convolution of Gaussian functions cantred at the calculated excitation energies by using the GaussSum[65] (version 2.2.4) software. The Chemcraft[66] program (version 1.6) was used for visualization of the computed results, including the representation of the geometries and the orbitals.

Supporting Information (see footnote on the first page of this article): The raw NMR spectroscopic data, optimized structures, an example of a simulated absorption spectrum, selected calculated structural data, β tensor components and orientational averages of the tensor components resulting from DFT calculations.

Acknowledgments

The authors thank the Fundação para a Ciência e Tecnologia (FCT) for funding (project number FCOMP-01-0124-FEDER-007433). T. J. L. S. is also grateful to the FCT for his Ph.D. grant.

[1] D. J. Williams, *Angew. Chem.* **1984**, *96*, 637; *Angew. Chem. Int. Ed. Engl.* **1984**, *23*, 690–703.
[2] H. S. Nalwa, *Appl. Organomet. Chem.* **1991**, *5*, 349–377.
[3] N. J. Long, *Angew. Chem.* **1995**, *107*, 37; *Angew. Chem. Int. Ed. Engl.* **1995**, *34*, 21–38.
[4] T. Verbiest, S. Houbrechts, M. Kauranen, K. Clays, A. Persoons, *J. Mater. Chem.* **1997**, *7*, 2175–2189.
[5] I. R. Whittall, A. M. McDonagh, M. G. Humphrey, M. Samoc, *Organometallic Complexes*, in: *Nonlinear Optics, I: Second-Order Nonlinearities*, in: *Advances in Organometallic Chemistry* (Eds.: F. G. A. Stone, W. Robert), Elsevier Inc., **1998**, vol. 42, p. 291–362.
[6] S. Di Bella, *Chem. Soc. Rev.* **2001**, *30*, 355–366.
[7] E. Goovaerts, W. E. Wenseleers, M. H. Garcia, G. H. Cross, *Design and characterization of organic and organometallic molecules for second order non-linear optics*, in: *Handbook of Advanced Electronic and Photonic Materials and Devices* (Ed.: H. S. Nalwa), Academic Press, Burlington, **2001**, p. 127–191
[8] C. E. Powell, M. G. Humphrey, *Coord. Chem. Rev.* **2004**, *248*, 725–756.
[9] E. Cariati, M. Pizzotti, D. Roberto, F. Tessore, R. Ugo, *Coord. Chem. Rev.* **2006**, *250*, 1210–1233.
[10] H. Bozec, V. Guerchais, *Molecular Organometallic Materials for Optics*. Springer, Berlin, Heidelberg, **2010**, p. 230.
[11] J. Heck, M. Dede, *Ferrocene-Based Electro-Optical Materials*, in: *Ferrocenes*, Wiley, New York, **2008**, p. 319–392.
[12] M. H. Garcia, P. Florindo, M. F. M. Piedade, M. T. Duarte, M. P. Robalo, E. Goovaerts, W. Wenseleers, *J. Organomet. Chem.* **2009**, *694*, 433–445.
[13] M. H. Garcia, P. J. Mendes, M. P. Robalo, M. T. Duarte, N. Lopes, *J. Organomet. Chem.* **2009**, *694*, 2888–2897.
[14] M. H. Garcia, P. J. Mendes, M. P. Robalo, A. R. Dias, J. Campo, W. Wenseleers, E. Goovaerts, *J. Organomet. Chem.* **2007**, *692*, 3027–3041.
[15] M. H. Garcia, M. P. Robalo, A. R. Dias, M. F. M. Piedade, A. Galvão, W. Wenseleers, E. Goovaerts, *J. Organomet. Chem.* **2001**, *619*, 252–264.
[16] W. Wenseleers, E. Goovaerts, P. Hepp, M. H. Garcia, M. P. Robalo, A. R. Dias, M. F. M. Piedade, M. T. Duarte, *Chem. Phys. Lett.* **2003**, *367*, 390–397.
[17] M. H. Garcia, M. P. Robalo, A. R. Dias, M. T. Duarte, W. Wenseleers, G. Aerts, E. Goovaerts, M. P. Cifuentes, S. Hurst, M. G. Humphrey, M. Samoc, B. Luther-Davies, *Organometallics* **2002**, *21*, 2107–2118.
[18] W. Wenseleers, W. Gerbrandij, E. Goovaerts, M. H. Garcia, M. P. Robalo, M. J. Mendes, C. J. Rodrigues, R. A. Dias, *J. Mater. Chem.* **1998**, *8*, 925–930.
[19] B. J. Coe, *Chem. Eur. J.* **1999**, *5*, 2464–2471.
[20] I. Asselberghs, K. Clays, A. Persoons, M. D. Ward, J. McCleverty, *J. Mater. Chem.* **2004**, *14*, 2831–2839.
[21] B. J. Coe, *Acc. Chem. Res.* **2006**, *39*, 383–393.
[22] K. A. Green, M. P. Cifuentes, M. Samoc, M. G. Humphrey, *Coord. Chem. Rev.* **2011**, *255*, 2530–2541.
[23] F. Mançois, J.-L. Pozzo, J. Pan, F. Adamietz, V. Rodriguez, L. Ducasse, F. Castet, A. Plaquet, B. Champagne, *Chem. Eur. J.* **2009**, *15*, 2560–2571.
[24] M. Moreno Oliva, J. Casado, J. T. López Navarrete, G. Hennrich, M. C. Ruiz Delgado, J. Orduna, *J. Phys. Chem. C* **2007**, *111*, 18778–18784.
[25] Y. Liu, G.-C. Yang, C.-G. Liu, S.-L. Sun, Y.-Q. Qiu, *Int. J. Quantum Chem.* **2012**, *112*, 779–788.
[26] B. Champagne, A. Plaquet, J.-L. Pozzo, V. Rodriguez, F. Castet, *J. Am. Chem. Soc.* **2012**, *134*, 8101–8103.
[27] C.-H. Wang, N. N. Ma, X.-X. Sun, S.-L. Sun, Y.-Q. Qiu, P.-J. Liu, *J. Phys. Chem. A* **2012**, *116*, 10496–10506.
[28] S. Di Bella, I. P. Oliveri, A. Colombo, C. Dragonetti, S. Righetto, D. Roberto, *Dalton Trans.* **2012**, *41*, 7013–7016.
[29] C.-G. Liu, Z.-M. Su, X.-H. Guan, S. Muhammad, *J. Phys. Chem. C* **2011**, *115*, 23946–23954.
[30] G. R. Hutchison, M. A. Ratner, T. J. Marks, *J. Phys. Chem. B* **2005**, *109*, 3126–3138.
[31] Y. Qin, J. Y. Kim, C. D. Frisbie, M. A. Hillmyer, *Macromolecules* **2008**, *41*, 5563–5570.
[32] A. Drury, S. Burbridge, P. A. Davey, J. W. Blau, *J. Mater. Chem.* **1998**, *8*, 2353–2355.
[33] R. D. A. Hudson, I. Asselberghs, K. Clays, L. P. Cuffe, J. F. Gallagher, A. R. Manning, A. Persoons, K. Wostyn, *J. Organomet. Chem.* **2001**, *637–639*, 435–444.
[34] P. J. Mendes, T. J. L. Silva, M. H. Garcia, J. P. P. Ramalho, A. J. P. Carvalho, *J. Chem. Inf. Comput. Sci.* **2012**, *52*, 1970–1983.
[35] R. H. L. Kiebooms, P. J. A. Adriaensens, D. J. M. Vanderzande, J. M. J. V. Gelan, *J. Org. Chem.* **1997**, *62*, 1473–1480.
[36] P. Amaladass, J. A. Clement, A. K. Mohanakrishnan, *Eur. J. Org. Chem.* **2008**, 3798–3810.
[37] A. K. Mohanakrishnan, P. Amaladass, *Tetrahedron Lett.* **2005**, *46*, 4225–4229.
[38] L. l. Bonniard, S. Kahlal, A. K. Diallo, C. t. Ornelas, T. Roisnel, G. Manca, J. o. Rodrigues, J. Ruiz, D. Astruc, J.-Y. Saillard, *Eur. J. Inorg. Chem.* **2010**, *50*, 114–124.
[39] C. Ornelas, C. Gandum, J. Mesquita, J. Rodrigues, M. H. Garcia, N. Lopes, M. P. Robalo, K. Nättinen, K. Rissanen, *Inorg. Chim. Acta* **2005**, *358*, 2482–2488.
[40] G. Zotti, S. Zecchin, A. Berlin, S. Grimoldi, M. C. Pasini, M. M. M. Raposo, *Chem. Mater.* **2005**, *17*, 6492–6502.
[41] P. Hapiot, F. Demanze, A. Yassar, F. Garnier, *J. Phys. Chem.* **1996**, *100*, 8397–8401.
[42] J. L. Oudar, D. S. Chemla, *J. Chem. Phys.* **1977**, *66*, 2664–2668.
[43] A. Willetts, J. E. Rice, D. M. Burland, D. P. Shelton, *J. Chem. Phys.* **1992**, *97*, 7590–7599.
[44] T. Verbiest, K. Clays, V. Rodriguez, *Second-Order Nonlinear Optical Characterization Techniques – An Introduction*, CRC Press, New York, **2009**.
[45] L. Jensen, P. T. van Duijnen, *J. Chem. Phys.* **2005**, *123*, 074307–7.
[46] W. L. F. Armarego, C. L. L. Chai, *Purification of Laboratory Chemicals*, 5th ed., Butterworth-Heinemann, **2003**.

[47] G. S. Ashby, M. I. Bruce, I. B. Tomkins, R. C. Wallis, *Aust. J. Chem.* **1979**, *32*, 1003–1016.
[48] K. Willinger, K. Fischer, R. Kisselev, M. Thelakkat, *J. Mater. Chem.* **2009**, *19*, 5364–5376.
[49] N. G. Connelly, W. E. Geiger, *Chem. Rev.* **1996**, *96*, 877–910.
[50] S. Stadler, R. Dietrich, G. Bourhill, C. Bräuchle, A. Pawlik, W. Grahn, *Chem. Phys. Lett.* **1995**, *247*, 271–276.
[51] J. Ipaktschi, J. Mohseni-Ala, A. Dülmer, S. Steffens, C. Wittenburg, J. Heck, *Organometallics* **2004**, *23*, 4902–4909.
[52] C. Lambert, G. Nöll, E. Schmälzlin, K. Meerholz, C. Bräuchle, *Chem. Eur. J.* **1998**, *4*, 2129–2135.
[53] R. Bersohn, Y.-H. Pao, H. L. Frisch, *J. Chem. Phys.* **1966**, *45*, 3184–3198.
[54] D. A. Kleinman, *Phys. Rev.* **1962**, *126*, 1977–1979.
[55] S. J. Cyvin, J. E. Rauch, J. C. Decius, *J. Chem. Phys.* **1965**, *43*, 4083–4095.
[56] M. J. Frisch, G. W. Trucks, H. B. Schlegel, G. E. Scuseria, M. A. Robb, J. R. Cheeseman, G. Scalmani, V. Barone, B. Mennucci, G. A. Petersson, H. Nakatsuji, M. Caricato, X. Li, H. P. Hratchian, A. F. Izmaylov, J. Bloino, G. Zheng, J. L. Sonnenberg, M. Hada, M. Ehara, K. Toyota, R. Fukuda, J. Hasegawa, M. Ishida, T. Nakajima, Y. Honda, O. Kitao, H. Nakai, T. Vreven, J. A. Montgomery, J. E. Peralta, F. Ogliaro, M. Bearpark, J. J. Heyd, E. Brothers, K. N. Kudin, V. N. Staroverov, R. Kobayashi, J. Normand, K. Raghavachari, A. Rendell, J. C. Burant, S. S. Iyengar, J. Tomasi, M. Cossi, N. Rega, J. M. Millam, M. Klene, J. E. Knox, J. B. Cross, V. Bakken, C. Adamo, J. Jaramillo, R. Gomperts, R. E. Stratmann, O. Yazyev, A. J. Austin, R. Cammi, C. Pomelli, J. W. Ochterski, R. L. Martin, K. Morokuma, V. G. Zakrzewski, G. A. Voth, P. Salvador, J. J. Dannenberg, S. Dapprich, A. D. Daniels, Ö. Farkas, J. B. Foresman, J. V. Ortiz, J. Cioslowski, D. J. Fox, *Gaussian 09*, rev. A.01, Gaussian, Ltd., Wallingford, CT, **2009**.
[57] T. Yanai, D. P. Tew, N. C. Handy, *Chem. Phys. Lett.* **2004**, *393*, 51–57.
[58] P. J. Hay, W. R. Wadt, *J. Chem. Phys.* **1985**, *82*, 270–283.
[59] P. J. Hay, W. R. Wadt, *J. Chem. Phys.* **1985**, *82*, 299–310.
[60] C. E. Check, T. O. Faust, J. M. Bailey, B. J. Wright, T. M. Gilbert, L. S. Sunderlin, *J. Phys. Chem. A* **2001**, *105*, 8111–8116.
[61] D. Feller, *J. Comput. Chem.* **1996**, *17*, 1571–1586.
[62] K. L. Schuchardt, B. T. Didier, T. Elsethagen, L. Sun, V. Gurumoorthi, J. Chase, J. Li, T. L. Windus, *J. Chem. Inf. Comput. Sci.* **2007**, *47*, 1045–1052.
[63] R. Nalewajski, *Density Functional Theory*, in: *Perspectives in Electronic Structure Theory*, Springer, Berlin, Heidelberg, **2011**, p. 255–368.
[64] M. E. Casida, C. Jamorski, K. C. Casida, D. R. Salahub, *J. Chem. Phys.* **1998**, *108*, 4439–4449.
[65] N. M. O'Boyle, A. L. Tenderholt, K. M. Langner, *J. Comput. Chem.* **2008**, *29*, 839–845.
[66] http://www.chemcraftprog.com.

Received: January 16, 2013
Published Online: May 31, 2013

